A numerical model for masonry implemented in the framework of a discrete formulation

A. Nappi†

Department of Civil Engineering, University of Trieste, P.le Europa 1, 34127 Trieste, Italy

F. Tin-Loi†

*School of Civil and Environmental Engineering, The University of New South Wales,
Sydney 2052, Australia*

Abstract. A direct discrete formulation suitable for the nonlinear analysis of masonry structures is presented. The numerical approach requires a pair of dual meshes, one for describing displacement fields, one for imposing equilibrium. Forces and displacements are directly used (instead of having to resort to a model derived from a set of differential equations). Associated and nonassociated flow laws are dealt with within a complementarity framework. The main features of the method and of the relevant computer code are discussed. Numerical examples are presented, showing that the numerical approach is able to describe plastic strains, damage effects and crack patterns in masonry structures.

Key words: crack growth; damage mechanics; discrete formulation; linear complementarity problems; masonry; mathematical programming; nonlinear structural analysis; plasticity.

1. Introduction

During the last decades masonry has been the object of large scale research activities. After initial descriptions based on the concept of *no-tension material* (Panzeca and Polizzotto 1988, Maier and Nappi 1985), models were developed by introducing adequate strength criteria (Page 1978, Benedetti and Benzoni 1984, Dhanasekar *et al.* 1985, Lofti and Shing 1991, Tomazevic and Weiss 1994, Gambarotta and Lagomarsino 1997, Nappi *et al.* 1997, Lourenço *et al.* 1998, Molins and Roca 1998). Homogenisation techniques were also applied, in spite of some limitations (Pande *et al.* 1989, Maier, Nappi and Papa 1991, Papa 1996). General overviews are given by Maier, Papa and Nappi 1991 and Lourenço 1996.

Numerical techniques applied to masonry structures and presented in the literature are mostly concerned with finite element discretisations. In this paper, we follow a non-traditional discrete formulation that is applicable to a wide range of physical theories (Tonti 2000A and 2000B), is based on two dual meshes, allows one to derive governing equations in a simple form and takes into account the intrinsic features of the measurable physical quantities (such as displacements and forces in solid mechanics) keeping their roles strictly separate. The discrete formulation is combined

---

† Professor

with a numerical material model specifically developed for masonry. It is suitable for describing some essential features of brick masonry and only requires a few parameters, whose values may be estimated even in the case of ancient buildings. Indeed, it takes into account joint slip and brick fracture, limited to the description of vertical cracks.

Slips and/or cracks are assumed to take place along horizontal and/or vertical interfaces along which internal forces are mutually exchanged. Horizontal interfaces are representative of mortar beds, while vertical interfaces are related to vertical joints and/or surfaces along which brick cracks may develop. Inelastic phenomena require the introduction of one surface (quite analogous to the yield surface in plasticity) that bounds the elastic domain. When loads along interfaces attain convenient values, cracks are allowed to develop. In this case, a softening behaviour is enforced. By introducing piecewise linear approximations of the critical surface and of the softening rule, a linear complementarity problem is derived. When cracks start to open, tensile stresses along crack surfaces tend to decrease (owing to development of the so called *process zone*) till they eventually become zero. In this case, deformations associated to fractures are to be assumed as reversible, since crack closure may occur. This fact essentially implies a nonlinear elastic behaviour, that is easily described through a proper formulation of the linear complementarity problem.

In the following sections the general theoretical background will be discussed and some details will be given on computational aspects. Finally, numerical tests will be presented to illustrate the main features of the results to be expected in terms of crack patterns.

2. A discrete formulation

A numerical approach is outlined, by using a discrete formulation and by maintaining a clear distinction between *configuration variables* (displacements) and *source variables* (external tractions, body forces and loads exchanged along internal interfaces). To this aim, a double mesh is required, as schematically shown in Fig. 1 with reference to plane problems. The first mesh, assumed as *primal* and shown by thick lines, consists of rectangles, such as *ABCD*, fully analogous to four-node finite elements. Inside each rectangle, a displacement field can be introduced that depends upon the vertex displacements. The second, *dual* mesh (thin lines) also consists of rectangles. Three of them are pointed out by means of shaded areas. When they are inside the given domain (such as *EFGH*), their vertices coincide with the centres of gravity of the primal rectangles. Otherwise, one or more vertices are at the middle of boundary sides of the primal mesh. Typical examples are given by *JKLF* and *MNPQ*. Rectangles of the dual mesh are used for balance (equilibrium) equations, which are written by including body forces, internal tractions exchanged along interfaces and external tractions. For instance, body forces and internal tractions are required for rectangles such as *EFGH*, while *JKLF* and *MNPQ* require also external tractions (whose values are obviously zero if boundary sides are not loaded).

It is worth noting that different geometrical elements are considered for the primal and the dual mesh. This is consistent with the intrinsic nature of the state variables utilised with each mesh. It also reflects a basic feature of physical quantities, which are always related to appropriate geometrical quantities. Typical examples are given by temperature and point, heat flow and surface, mass and volume. In the specific (mechanical) case we are discussing, displacements are associated to vertices or other points of the primal mesh, while forces are related to volumes or surfaces (interfaces) of the dual mesh. It is well known that a clear distinction of this kind is often ignored
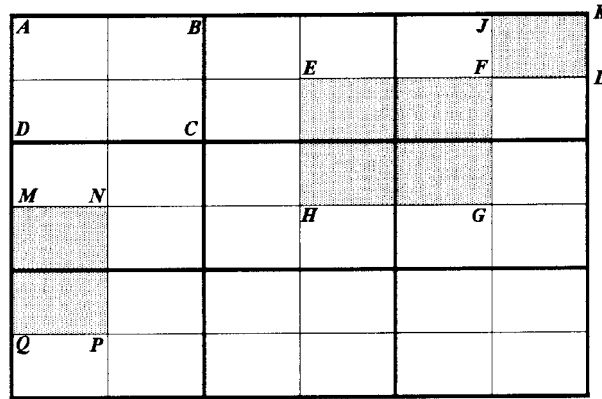
Fig. 1 Primal and dual mesh

(e.g., equivalent nodal loads are *fictitious* forces applied at significant points of finite element models). It is obviously true that concentrated loads have been traditionally used for a long time and that forces are often associated to an *application point*, but this is a rather crude approximation, quite useful when particles are discussed. However, both particles and concentrated forces represent abstract concepts. This statement is simply proved, in the case of loads, by the fact that forces are measurable quantitities and there is no way, in practice, of measuring loads concentrated at points.

For each rectangle of the primal mesh (e.g., *ABCD* in Fig. 1) a bilinear displacement field is assumed, that depends upon vertex displacements. The displacement gradient and, hence, the strain distribution must be considered inside each primal cell.

Next, we start to consider the dual mesh in order to impose equilibrium. Although it is not strictly necessary at this stage, we may subdivide each primal rectangle into four triangles (cf. Fig. 2). As discussed later, these triangles will be utilised as subregions where inelastic strains may be smeared. In any case, for each dual rectangle without boundary sides, such as *EFGH* in Fig. 1, it is now possible to identifiy eight portions of the interfaces that belong to eight different triangles. The eight portions are obviously shown by segments in Fig. 2. It is understood, however, that they represent interfaces characterised by their own surfaces A_m ($m=1, ..., 8$). In view of the bilinear displacement field, a linear distribution of strains occurs along each segment. Consequently, if the material behaviour is elastic, along each segment there exists a linear stress field. By assuming the usual pair
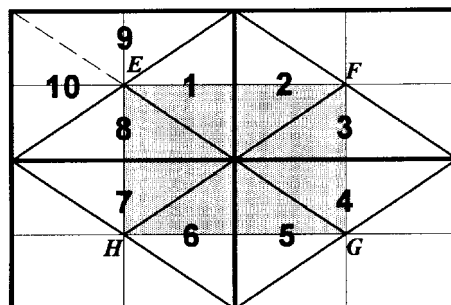

Fig. 2 Dual cell and relevant triangles

of Cartesian orthogonal axes x (horizontal) and y (vertical), the stress components σ_{yy} and σ_{xy} along any horizontal segment represent the normal and shear forces per unit surface exchanged through a certain interface. Similarly, in the case of vertical segments, such forces correspond to the stress components σ_{xx} and σ_{xy}. Since the stress distribution is linear along each segment, products such as $\{R_m s_m A_m\}$ immediately provide the resultant forces (no summation implied). Here, R_m is a rotation matrix and s_m is the stress vector that collects the three stress components σ_{xx}, σ_{yy}, σ_{xy} at the middle of the m-th segment. It is quite obvious that R_m is a 2×3 matrix, since we need to transform the stress components into the normal and shear forces per unit surface exchanged through an interface.

It is now possible to write one balance (equilibrium) equation for each dual rectangle by setting

$$\Sigma_{m=1,\dots,8}\, R_m s_m A_m + F_B = 0 \tag{1}$$

where F_B denotes the body force acting on the current rectangle.

When dual rectangles are along the boundary (for instance, *JKLF* and *MNPQ* in Fig. 1) a lower number of triangles, say T, will be used (e.g., $T=2$ and $T=4$ for *JKLF* and *MNPQ*). In addition, proper surface forces F_S shall be introduced into the equilibrium equation to account for given external loads along the boundary. Thus, Eq. (1) becomes

$$\Sigma_{m=1,\dots,T}\, R_m s_m A_m + F_B + F_S = 0 \tag{2}$$

Stresses can be expressed as functions of strains, and strains, in turn, as functions of four primal displacement vectors (those concerned with the nodes of the primal cell to which the current segment interface belongs). If the material is assumed to be linear elastic, this operation is carried out quite easily and a linear system of equations is derived. This system is formally analogous to the one found with finite elements (e.g., $Ku=Q$, if u collects displacement components of the nodes of the primal mesh, while Q is related to body and surface forces acting upon dual cells).

Inelastic problems, however, can also be considered. To this aim, we may introduce linear distributions of inelastic strains along the interfaces of the dual cells. Alternatively, constant inelastic strains may be assumed within each triangle that represents one subdivision of a primal cell. An example is given by the cell in Fig. 2 subdivided into the triangles 1, 8, 9, 10. We shall follow this approach and will enforce the constitutive law at the mid point of each segment. Thus, by introducing the inelastic strain vector e_m^I at each triangle ($m=1, \dots, T^*$, with $T^* \leq 8$), the stress vector in Eq. (1) or (2) becomes $s_m = D_m(e_m - e_m^I)$, where D_m is the material stiffness matrix and e_m the vector of total strains. In view of this relationship, by expressing strains as functions of primal displacements the equilibrium Eqs. (1) and (2) lead to

$$Ku + Lw = Q \tag{3}$$

Here, w collects all the inelastic strain vectors e_m^I. By combining Eq. (3) with appropriate constitutive laws, *step-by-step* solutions of incremental problems can be found.

3. A numerical model for masonry

The discrete formulation discussed in the previous Section has been applied to the numerical analysis of masonry, described as a macroscopically homogeneous material (without considering the mechanical properties of mortar and bricks or stones separately). Let us focus, for instance, on the masonry assembly of Fig. 3 subjected to the uniform tractions N_x, N_y and S. It may be represented
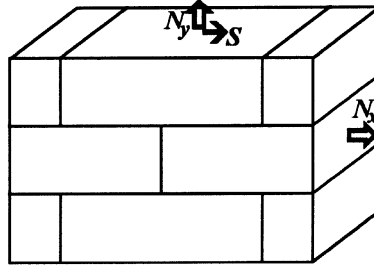
Fig. 3 Typical brickwork

by a macroscopically homogeneous discrete model (such as the simple one represented in Fig. 2). Then, joint slips can be described by assuming that they may occur along the interfaces of the primal cells (e.g., segments 1-8 in Fig. 2). This can be done by introducing an adequate criterion (such as Mohr-Coulomb's condition) and by defining a convenient yield surface in the space N_x-N_y-S. So far, we have considered piecewise linear approximations of the surface. An example is given in Fig. 4, that shows the intersections of seven yield planes with the plane N_y-S (which is of interest for horizontal interfaces). Similar intersections may be considered in the plane N_x-S for vertical joints. The circle in Fig. 4 corresponds to the limit stress state for joints subjected to tensile loads.

Similarly, fracture processes in bricks may be assumed along vertical interfaces (*e.g.*, segments 3, 4, 7, 8 in Fig. 2). Thus, further inelastic strains (corresponding to cracks in bricks) are allowed to develop along these interfaces, when brick elongations (i.e., tractions N_x and N_y) attain critical values. Consequently, the relevant yield surface consists of one additional plane, whose projection on the N_x-N_y plane is shown in Fig. 5 with a thick line. The thin line has no interest in this context, since it refers to values of N_x and N_y for which horizontal cracks might occur. Obviously, an approximation is introduced, since brick cracks, in principle, may have any orientation. It is true, however, that vertical or nearly vertical cracks are usually dominant in bricks, so that significant errors are not introduced by this assumption. On the other hand, a numerical model has been obtained, that is able to describe the main features of masonry by considering a small number of possible failure modes (slips or cracks at joints and vertical cracks in bricks). This choice seems to represent a reasonable compromise between the advantages of a simple description and a satisfactory
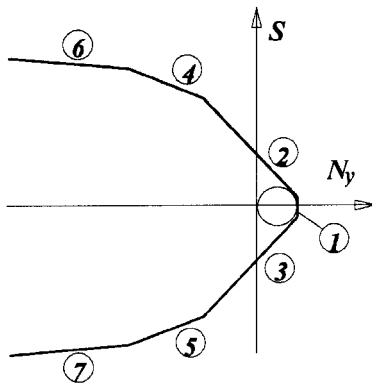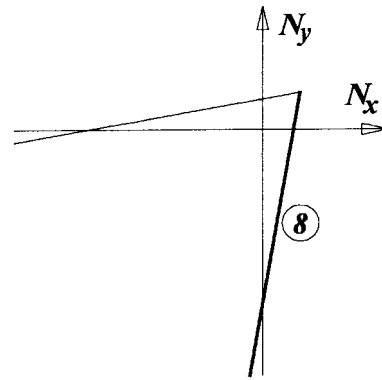

Fig. 4 Yield planes 1-7

Fig. 5 Yield plane 8

level of accuracy. Indeed, the model appears suitable for practical applications, since limited experimental information is required: joint strength and critical brick elongation. It is worth noting that such parameters can be estimated, at least to some extent, even in the case of old historical buildings.

4. Some computational aspects

The model discussed here implies crack effects smeared throughout a certain volume element. Displacement discontinuities are not explicitly considered. Consequently, when the relative displacement d between two points is partially due to crack opening, the portion of d related to inelastic effects is given by $\varepsilon^* L^*$, where ε^* denotes one inelastic strain component and L^* is a characteristic length. Therefore, mechanical properties are derived from experimental data in terms of forces and displacements measured in masonry units (subject to macroscopically homogeneous stress states). Next, critical values of interface loads are found by considering the dimensions of primal cells.

Let us consider, for instance, a shear test that implies a relative horizontal displacement between the upper and the lower edge of one masonry unit. The inelastic part (say η) of the displacement can be associated to an inelastic strain ε_{xy}^I such that $\eta = 2h\varepsilon_{xy}^I$, where h is the height of the test specimen.

If we consider uniaxial tension, we may focus on the fracture energy E_F required to develop a major crack, such as a horizontal crack through a whole masonry unit. In this case, at the end of the crack propagation process, no tensile strength is available along the vertical direction. A softening law can be defined so that the same energy E_F be found when ε^* attains the value at which the normal stress becomes zero. In this way, mesh dependent results (quite typical with softening) may be avoided (cf. Bazant and Cedolin 1979). For instance, if h is again the height of the masonry unit and δ^* represents the crack opening at the end of the process (exactly when the softening branch is over and the tensile strength becomes zero), the critical value ε^* shall correspond to the ratio δ^*/h.

The approach described so far, may give non-desired effects owing to inelastic strains that are uniform throughout triangular regions. Let us consider, for instance, one rectangular wall subject to uniform downwards displacements at the top, while zero vertical displacements are imposed at the bottom and horizontal displacemens are not constrained anywhere. When the compression stress is sufficiently high, vertical cracks should develop (for instance along the vertical interfaces of the dual cells that make up the discrete model of Fig. 2). Since the effects of these cracks are described by means of smeared inelastic strains ε_{xx}^I, such strains should be uniform. However, on the basis of the yield surfaces introduced in the previous Section, only triangles such as 3, 4, 7, 8, 9 in Fig. 2 may be subjected to inelastic strains, since a critical value of the force N_y (cf. Fig. 5) can only occur along the vertical interfaces. On the other hand, triangles such as 1, 2, 5, 6 and 10 remain in the elastic range. Consequently, horizontal stresses σ_{xx} (not consistent with the real behaviour) are generated in these triangles. The problem is removed by imposing that an inelastic strain vector e_k^I in the k-th triangle enforce an inelastic strain vector equal to $\{\frac{1}{2} \ e_k^I\}$ in the adjacent triangles that belong to the same primal cell. Thus, inelastic strains ε_{xx}^I in triangles such as 8 and/or 9 imply inelastic strains $(\frac{1}{2} \ \varepsilon_{xx}^I)$ in 1 and 10. In this way, the total additional inelastic strain in 1 and 10 equals ε_{xx}^I if both 8 and 9 are affected by the inelastic strain ε_{xx}^I.

By following this approach, inelastic strains ε_{xx}^I were correctly computed for one rectangular wall, whose primal mesh is shown in Fig. 6 by thin lines. As pointed out above, a uniform stress field
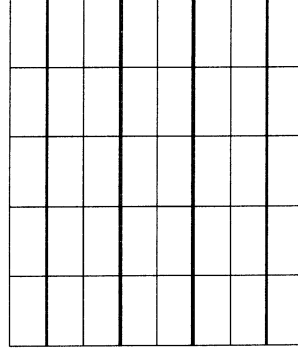
Fig. 6 Brickwork subjected to uniform compression and relevant crack pattern

was obtained by constraining vertical displacements along the bottom edge and imposing equal downward displacements on top. As the stress attained a critical value, the eighth mode (cf. Fig. 5) became active and uniform inelastic strains ε_{xx}^I started to develop. Such strains may be interpreted as smeared strains that actually correspond to displacement discontinuities along the vertical interfaces located between dual cells. At this stage the crack pattern is easily identified: for instance, thick lines (cf. Fig. 6) may be used to represent interfaces subjected to inelastic strains which are associated to the eighth plastic mode.

Since the elastic domain is bounded by seven or eight planes at each interface, the inelastic strains of each primal cell are found through an equation such as $e^I=mz$, where z contains thirty plastic multipliers (one for each plane). The vector e^I collects four subvectors e_k^I ($k=1, ..., 4$) that consist of the entries ε_{xx}^I, ε_{yy}^I, γ_{xy}^I. The matrix m is so defined that any inelastic strain ε^I in the k-th triangle (e.g., 1 in Fig. 2) implies a strain ($\frac{1}{2} \varepsilon^I$) in the contiguous triangles (e.g., 8 and 9). At this stage, we can introduce the vector S that collects the subvectors $S_k=D_kA_k(e_k-e_k^I)$. Here, D_k is the stiffness matrix of the k-th triangle ($k=1, ..., 4$) and e_k is the strain vector at the mid point of the interface portion inside the same triangle. The term A_k denotes a diagonal matrix whose non-zero entries are $A_k=t_kl_k$, where ($t_k l_k$) represents the product between the thickness and the length of the interface portion inside the k-th triangle (i.e., the area of such portion). The vector S can also be expressed in incremental terms. By introducing the vector S_o that denotes the stresses at the beginning of the current time-step, we obtain $S=S_o+D\{\Delta e-m\Delta z\}$, where D is the block diagonal matrix diag$[D_kA_k]$, with no summation implied. Thus, for each primal cell we obtain

$$y=n^TS_o+n^T D\{\Delta e-m \Delta z\}-r \leq 0, \ \Delta z \geq 0, \ y^T\Delta z=0 \tag{4a-c}$$

Here, the vector r collects the distances of the yield planes from the origins of the spaces in which they are defined. Of course, thirty distances are required for each primal cell (e.g., seven planes for the triangles 1 and 10 in Fig. 2, eight planes for the triangles 8 and 9). The matrix n, instead, is made of outward unit vectors which are normal to the yield planes and project the stress vectors along the directions which are normal to the yield planes. The complementarity constraint (4c) implies non-zero inelastic strains whenever at least one yield plane is violated. The above relationships, to be satisfied for each cell, allow us to perform a nonlinear step-by-step analysis of masonry. To this aim, such relationships must be combined with Eq. (4) or its counterpart written in incremental terms: $K \Delta u+L\Delta w =\Delta Q$ (Maier 1970 and Cottle *et al.* 1992).

For a proper description of masonry behaviour, a hardening/softening rule is needed for the yield

planes by introducing a convenient function $r = r\,(\Delta z)$. For the sake of simplicity, single softening branches have been considered (*cf.* Fig. 7). Therefore, a piecewise-linear approximation has been adopted for each entry, say $r = r(\Delta\lambda)$, of the vector ***r***. The relatively simple plot of Fig. 7, is characterised either by the softening branch (a) or by the horizontal branch (b). Branches such as (a) are assumed at the beginning of the load history. Later, if the distance of one plane from the origin becomes zero, the branch (b) is utilised for that plane.

It is worth noting that more complex relationships (involving multi-branch softening curves) may be taken into account.

Some examples of such softening laws, albeit not necessarily related to fracture but still entirely applicable, have been proposed recently by Tin-Loi and Ferris (1997) and Tin-Loi and Xia (2000). It should be noted that, in the present stepwise approach where each step is assumed to be fully reversible (or holonomic), proper descriptions of such holonomic softening laws are not entirely straightforward. The seminal work in this direction was carried out by Bolzon *et al.* (1994) who derived their two-branch piecewise linear softening model on the basis of mechanical considerations of contact and spring devices. It may be possible, within the present context, to assume simpler, quite acceptable but approximate laws involving an essentially diagonal softening matrix. This aspect, however, requires further investigation.

The linear r-$\Delta\lambda$ plot of Fig. 7 implies $r = r_o + H\Delta z$, with ***H*** constant, and makes Eqs. (4) define a *linear complementarity problem*. When ***H*** is given, the structural problem can be solved by an iterative prediction/correction process for each increment ΔQ:

(i) at the beginning of each step, we set $\Delta w = \mathbf{0}$ and Δu is found such that $\mathbf{K}\Delta u + \mathbf{L}\Delta w = \Delta Q$;

(ii) for each primal cell, increments Δe are computed and the problem (4) is solved;

(iii) the vector Δw is updated, a new increment Δu is found such that $\mathbf{K}\Delta u + \mathbf{L}\Delta w = \Delta Q$ and the process continues from point (ii) until the difference between the norms of Δw (or any other significant vector) at two subsequent iterations does not exceed a given tolerance;

(iv) The vector ***r*** is updated and the subsequent increment ΔQ is considered.

So far, numerical tests have been carried out by assuming a partial interaction between yield planes. To this aim, block diagonal ***H*** matrices have been assumed. More specifically, 2×2 blocks have been used for symmetric yield planes (2 and 3, 4 and 5, 6 and 7 in Fig. 4). Single diagonal entries have been used for planes 1 (cf. Fig. 4) and 8 (cf. Fig. 5), excluding any interaction with other planes. Equal entries have been assumed for 2×2 blocks. Thus, during a given time step, the same translation is imposed to the planes that belong to a certain pair. At the end of each time step the entries of ***r*** are updated even when the relevant inelastic modes have not been activated during the load increment. In other words, it is assumed that any reduction of strength (implied by the translation of one plane) also affects other inelastic modes. Consequently, at the end of each step, the minimum ratio r/r_o is considered for each triangle (cf. Fig. 2) and is usually imposed to all the
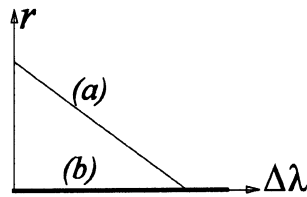

Fig. 7 r vs $\Delta\lambda$ plot

other planes concerned with the same triangle. Exceptions are found when that ratio would enforce a translation of one plane which is not consistent with the stress level determined at the end of the last time step. In this case the largest translation is enforced which is consistent with the current stress.

Thus, damage is taken into account by imposing a progressive decrease of the strength. The model may be enhanced by considering some loss of stiffness related to inelastic strains. Indeed, the material compliance matrix (and, hence, the stiffness matrix) can be updated as inelastic strains increase (Nappi *et al.* 1997, Papa and Nappi 1997). So far, this option has not been implemented in the framework of the formulation discussed in the paper. However the stiffness of the system is affected by crack opening, as pointed out in what follows. This fact will also be evident when numerical tests will be discussed in the next Section.

The model has been implemented with the objective of considering possible effects due to crack closure. To this aim, we introduce a new vector, say Δz_o, for every primal cell characterised by one or more interfaces that have fully lost their tensile strength (zero distance of one or more planes from the origin). The only non-zero entries of that vector are the terms which denote plastic multipliers associated to the planes passing through the origin. Such terms are given the values attained by the multipliers at the end of the previous time step. Next, we consider the n_I interfaces where no plane passes through the origin and where at least one normal (positive) inelastic strain ε_k^N combined with a positive normal stress σ_k^N has been found at least once ($k=1, ..., 4$). Thus, we can define a vector q_o made of n_I entries q_j ($q_j=\varepsilon_j^N$ if $\sigma_j^N \geq 0$ and $q_j=0$ if $\sigma_j^N<0$). We also introduce the n_I by n_I diagonal matrix h^*. Its j-th non-zero entry is ($\sigma_j^*/\varepsilon_j^*$), if ε_j^* denotes the largest value ever attained by ε_j^N. Eventually, instead of (4), we may consider the problem

$$y=n^TS_o+n^TD\{\Delta e+Cq_o+m\Delta z_o-Cq-m\Delta z\}-r \leq 0, \quad \Delta z \geq 0, \quad y^T\Delta z=0 \tag{5a-c}$$

$$v=BS_o+BD\{\Delta e+Cq_o+m\Delta z_o-Cq-m\Delta z\}-h^*q \leq 0, \quad q \geq 0, \quad v^Tq=0 \tag{5d-f}$$

where C selects the entries of q_o in such a way that the effects of inelastic strains related to a certain interface be taken into account also in adjacent triangles (as discussed above). The matrix B selects those entries of the stress vector, which provide the n_I normal forces associated to the strain components ε_j^N. Obviously, both the constraints (5d-f) and the vector $\{Cq_o\}$ in the inequality (5a) will not be considered if q_o is empty. When conditions (5) are satisfied, the normal inelastic strains are progressively recovered if the corresponding total strains decrease. On the other hand, if normal total strains increase, the increments of the inelastic strains at the end of the current time step are given by $\{Cq+m\Delta z-Cq_o-m\Delta z_o\}$.

The problem (5) combined with the linear system $K\Delta u+L\Delta w=\Delta Q$ generalises the governing equations

$$\sigma_o+k(\Delta\varepsilon+\xi_o-\Delta\lambda-\xi)=\sigma, \; \sigma-h\;\Delta\lambda-\sigma^*=y \leq 0, \; \Delta\lambda \geq 0, \; y\Delta\lambda=0 \tag{6a-d}$$

$$\sigma-g\xi=v \leq 0, \; \xi \geq 0, \; v\xi=0 \tag{6e-g}$$

These equations govern the response of the mechanical system of Fig. 8a. The parameters ξ and g play the role of q and h^* in the problem (5). The mechanical model consists of three linear elastic springs (whose stiffness parameters are k, $h<0$, g), one rigid, perfectly plastic slip (with yield limit equal to σ^*) and one no-tension element characterised by reversible strains ξ (Nappi *et al.* 1997). The relevant $\sigma-\varepsilon$ plot is given in Fig. 8b. The dashed path in Fig. 8b, in principle, may be followed in view of conditions (6), but is avoided by setting $h=0$ when $\sigma=0$.
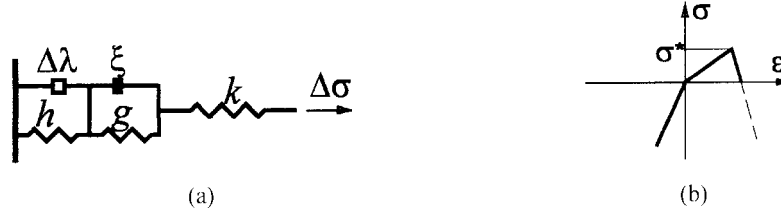
(a)   (b)

Fig. 8 (a) Mechanical model and (b) relevant $\sigma - \varepsilon$ plot

The meaning of Eqs. (6) may be easily understood by observing that the inequality (6e) practically enforces a linear hardening branch for $\sigma \geq 0$ (path in Fig. 8b characterised by positive stresses and positive slope). On the other hand, the inequality (6b) enforces a change of stiffness when the critical stress σ^* is attained. Obviously, for $h<0$, softening occurs.

5. Numerical tests

In order to test the numerical approach presented in the paper, some problems were solved using a simple implementation of Lemke's method (Cottle *et al.* 1992).

First, we paid some attention to the problem concerned with crack opening and closure. To this aim we considered the same brickwork discussed in the previous Section when we dealt with the crack pattern induced by compressive stresses. The wall was 1.5 m wide and a critical tensile stress equal to 1 MPa was assumed for mortar beds. A uniform stress field was imposed by enforcing vertical cyclic displacements to the top edge (path O-A-B-C-B-D-E-D-F-O-G in Fig. 9).

Top vertical forces per unit thickness (1 mm) are reported as functions of the vertical displacements (cf. Fig.9). It is quite clear that crack closure is taken into account, since the inelastic strains associated to the softening behaviour are reversible and tend to be recovered during unloading phases. Note that the global stiffness of the system highly depends on possible crack opening, as shown by the slopes of the paths *B-C*, *D-E* and *F-O*. When crack closure occurs, the initial stiffness is completely recovered (path *O-G*).
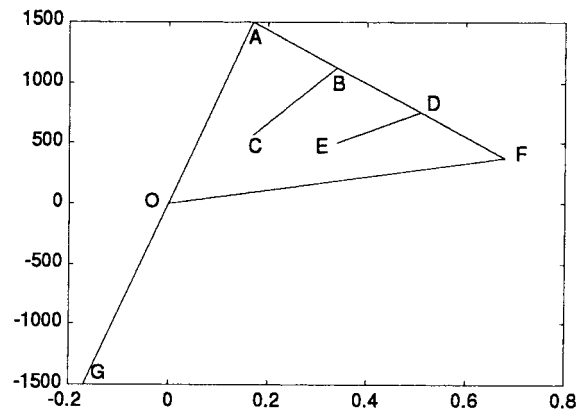

Fig. 9 Vertical force [N] vs displacement [mm] in the presence of uniform tensile stresses
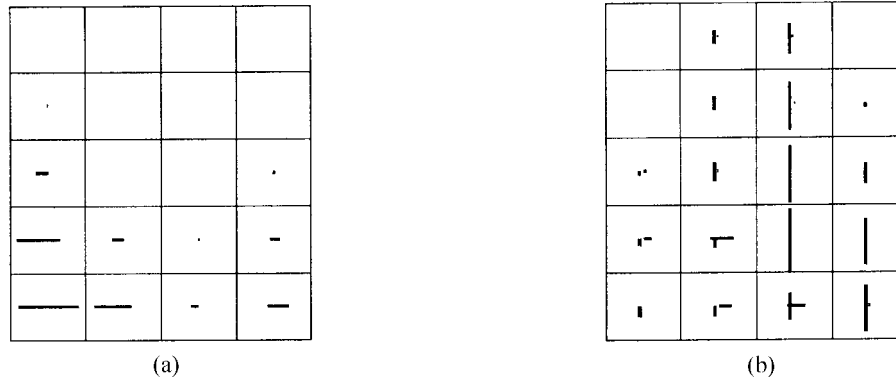
(a)   (b)

Fig. 10 Cracks due to (a) modes 1-3 and (b) modes 4-7

A further example is given in Fig. 10. A shear wall was discretised by 20 primal cells (length: 1.5 m, height 1.7 m, Young's modulus 10^4 MPa; Poisson's ratio: 0.15; brick tensile strength: 3 MPa; mortar tensile strength: 1 MPa). The wall was fully constrained at the bottom edge. The top edge was loaded by enforcing uniform compressive stresses (1 MPa). Next, cyclic horizontal displacements were imposed. As shown in Fig. 10, the computer code easily shows the crack pattern: thick, horizontal segments refer to cracks along mortar beds, while vertical lines are concerned with vertical joints. The length of segments is proportional to inelastic displacements and, hence, to crack opening. It is also possible to understand the type of crack by considering the plastic multipliers that are involved. For instance, Fig. 10a shows inelastic strains associated to planes 1-3 in Fig. 4. Thus, tensile stresses appear to be the main cause. On the other hand, cracks depicted in Fig. 10b are referred to modes 4-7 and are essentially due to shear loads, as suggested by their location. Since this numerical example involves one brickwork whose top edge is free to rotate, cracks due to tensile stresses are subjected to significant opening and closure effects. This is quite evident by considering the plot in Fig. 11, that gives the reaction shear force per unit thickness (1 mm) as a
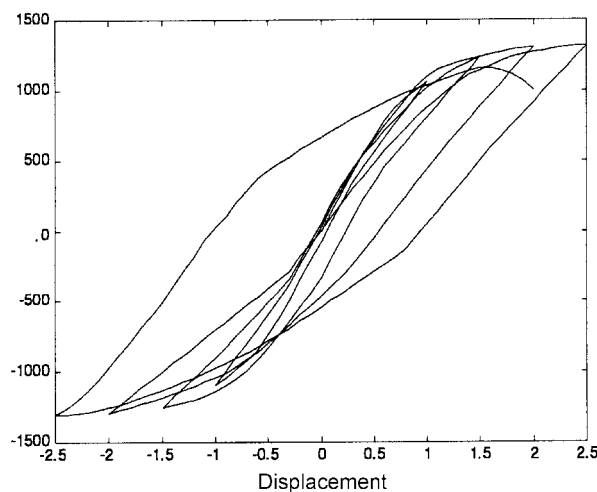

Fig. 11 Horizontal force [N] vs displacement [mm] for clamped wall with free top edge
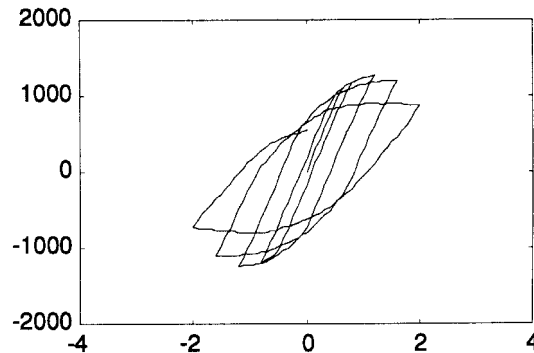
Fig. 12 Horizontal force [N] vs displacement [mm] for clamped-clamped brickwork

function of the horizontal displacement at the top. Several changes of slopes can be noted in the elastic range during unloading phases. They are clearly related to crack closure.

The last example is concerned with one brickwork discretised by sixty primal cells (length: 1.5 m; height: 2 m). The mechanical properties of the previous problem were considered. In this case the wall was clamped at the bottom and rotations were not allowed at the top. As before, a uniform compressive stress (1 MPa) was followed by cyclic horizontal displacements imposed along the top edge. A progressive reduction of strength can be noted, as typical of brickworks subjected to this kind of loads (cf. Fig. 12). Again, the reaction force is reported in the plot and is referred to a unit thickness (1 mm).

As already pointed out, a progressive decrease of stiffness should be introduced in order to enhance the model and to describe the actual masonry behaviour. However, the main features of masonry such as crack opening and closure, softening effects, progressive decrease of strength (cycle after cycle) appear to be properly described by the non traditional approch presented in the paper even in the present, simplified form.

6. Conclusions

A numerical approach to the analysis of masonry structures has been presented. It is based upon a discrete formulation that requires a dual mesh (one for configuration variables, one for source variables). The dual mesh spontaneously suggests the possibility of taking into account inelastic effects at joints and cracks in bricks by assuming that interfaces between dual cells may be interpreted as surfaces along which slips and/or detachments may occur. These effects are described by means of smeared inelastic strains fully analogous to the ones encountered in the framework of plasticity. The constitutive law has been enforced by solving linear complementarity problems since piecewise-linear yield surfaces and softening rules have been considered.

The approach is able to describe the essential features of masonry, including crack opening and closure (with consequent recovery of the initial stiffness when cracks are completely closed). A limited number of experimental parameters is required, so that the technique discussed in the paper does appear to be suitable for a significant range of practical applications.

Acknowledgements

References

Bazant, Z.P. and Cedolin, L. (1979), "Blunt crack band propagation in finite element analysis", *ASCE J. of Eng. Mech.*, **105**, 297-315.

Bolzon, G., Maier, G. and Novati, G. (1994), "Some aspects of quasi-brittle fracture analysis as a linear complementarity problem", *Fracture and Damage in Quasibrittle Structures*, Eds Z.P. Bazant, Z. Bittnar, M. Jirasek, J. Mazars, E&FN Spon, London, 159-174.

Cottle, R.W., Pang, J.S. and Stone, R.E. (1992), *The Linear Complementarity Problem*, Academic Press.

Benedetti, D. and Benzoni, G.M. (1984), "A numerical model for the seismic analysis of masonry buildings: Experimental correlations", *Earth. Eng. and Struct. Dyn.*, **12**, 817-831.

Dhanasekar, M., Kleeman, P.W. and Page, A.W. (1985), "Non-linear biaxial stress-strain relations for brick masonry", *ASCE J. of Struct. Div.*, **111**(5), 1085-1100.

Gambarotta, L. and Lagomarsino, S. (1997), "Damage models for the seismic response of brick masonry shear walls. Part II: The continuum model and its applications", *Earth. Eng. and Struct. Dyn.*, **26**(4), 441-462.

Lofti, H.R. and Shing, P.B. (1991), "An appraisal of smeared crack models for masonry shear wall analysis", *Comput. Struct.*, **41**, 413-425.

Lourenço, P.B. (1996), *Computational Strategies for Masonry Structures*, Delft University Press, Delft, The Netherlands.

Lourenço, P.B., Rots, J.G. and Blaauwendraad, J. (1998), "Continuum model for masonry: Parameter estimation and validation", *ASCE J. of Struct. Engineering*, **124**(6), 642-652.

Maier, G. (1970), "A matrix structural theory of piecewise-linear plasticity with interacting yield planes", *Meccanica*, **5**(1), 55-66.

Maier, G. and Nappi, A. (1985), "A theory of perfectly no-tension discretized structural systems", *Engineering Structures*, **12**, 227-234.

Maier, G., Nappi, A. and Papa, E. (1991), "Damage models for masonry as a composiste material: a numerical and experimental analysis", *Constitutive Laws for Engineering Materials,* Ed. by C.S. Desai, E. Krempl, G. Frantziskonis and H. Saadatmanesh, ASME Press, New York, 427-432.

G. Maier, E. Papa and A. Nappi (1991), "On damage and failure of brick masonry", *Experimental and Numerical Methods in Earthquake Engineering*, Ed. by J. Donea and P.M. Jones, ECSC, Brussels, 223-245.

Molins, C. and Roca, P. (1998), "Capacity of masonry arches and spatial frames", *ASCE J. of Struct. Engineering*, **124**(6), 653-663.

Nappi, A., Facchin, G. and Marcuzzi, C. (1997), "Structural dynamics: Convergence properties in the presence of damage and applications to masonry structures", *Structural Engineering and Mechanics*, **5**(5), 587-598.

Page, A.W. (1978), "Finite element model for masonry", *ASCE J. of Struct. Div.*, **104**, 1267-1285.

Pande, G.N., Liang, J.X. and Middleton, J. (1989), "Equivalent elastic moduli for brick masonry", *Computer and Geotechnics*, **8**, 243-265.

Panzeca, T. and Polizzotto, C. (1988), "Constitutive equations for no-tension materials", *Meccanica*, **23**, 88-93.

Papa, E. (1996), "A unilateral damage model for masonry based on a homogenization procedure", *Mechanics of Cohesive-Frictional Materials*, **1**, 349-366.

Papa, E. and Nappi, A. (1997), "Numerical modelling of masonry: A material model accounting for damage effects and plastic strains", *Applied Mathematical Modelling*, **21**(6), 319-335.

Tin-Loi, F. and Ferris, M.C. (1997), "Holonomic analysis of quasibrittle fracture with nonlinear softening", *Fracture Research*, Ed. by B.L. Karihaloo, Y.W. Mai, M.I. Ripley and R.O. Ritchie, Pergamon, 2183-2190.

Tin-Loi, F. and Xia, S.H. (2000), "Nonholonomic elastoplastic analysis involving unilateral frictionless contact as a mixed complementarity problem", *Computer Methods in Applied Mechanics and Engineering*, to appear.

Tomazevic, M. and Weiss, P. (1994), "Seismic behavior of plain and reiforced-masonry buildings", *ASCE J. of Struct. Engineering*, **120**, 2, 323-338.

Tonti, E. (2000A), "A finite formulation for the wave equation", *Journal of Computational Acoustics*, to appear.

Tonti, E. (2000B), "Finite formulation of electromagnetic field", *Journal of Electromagnetic Waves and Applications*, to appear.